metals

MDPI

Article

Analysis of Powder Binder Separation through Multiscale Computed Tomography

Shidi Yang [1], Qiaoli Xu [1,*], Chengcheng Liu [2], Xin Lu [2], Xuanhui Qu [2] and Ying Xu [3,*]

1 Tianjin Sanying Precision Instruments Co., Ltd., Tianjin 300399, China; sdyang@sypi.com.cn
2 Institute for Advanced Materials and Technology, University of science and technology Beijing, Beijing 100083, China; liu13907362319@163.com (C.L.); lu13907362319@163.com (X.L.); m15901296550@163.com (X.Q.)
3 School of Electromechanical Engineering, Guangdong University of Technology, Guangzhou 510006, China
* Correspondence: qlxu@sypi.com.cn (Q.X.); ying.xu@gdut.edu.cn (Y.X.); Tel.: +86-022-24874990 (Q.X.); +86-20-39322206 (Y.X.)

Received: 14 February 2019; Accepted: 8 March 2019; Published: 15 March 2019

check for updates

Abstract: In this study, X-ray computed tomography was used to analyze powder binder separation in TC4 green bodies. Firstly, for the scanned results of the whole green body, because of the relative low resolution (36 μm), the powder binder separation can only be analyzed by using gray value distribution. Then, local regions (areas near the gate and the central parts) were scanned by using a much higher resolution (2.3 μm). Both of the volume fraction of powder content and gray value distributions indicate that powder particles tend to accumulate in the central parts. Finally, based on the results tested by using submicron resolution (0.8 μm), the effects of the volume and morphology of the powder particles on the powder binder separation were analyzed.

Keywords: green body; powder binder separation; CT test; mold filling

1. Introduction

Powder injection molding (PIM) has an excellent ability to manufacture products with large quantities, low cost, complicated shape and excellent performance [1,2]. Thus, these products have been used to many industrial and research fields such as for automobile and aerospace parts. Four crucial steps are involved in PIM: feedstock made by mixing binder and powder particles, mold filling, binder removing from green body, and sintering of the powder particles [3]. The powder-binder separation phenomenon emerging in the mold filling is the major cause of nonhomogeneous composition distribution, which leads to the collapse and sagging of green body during debinding, as well as the geometrical error and non-uniform properties of the final sintered parts.

During mold filling, because of the physical property differences and pseudo-plastic behavior, the complex physical environments may lead to relative movement between the powder particles and binder. In the previous studies [4–8], much research was performed to analyze the powder-binder separation, and the characteristics of these methods were summarized in Table 1. It can be seen that an effective method for analyzing powder-binder separation of the green body nondestructively is urgently needed.

Recently, X-ray computed tomography has been widely applied to material science and engineering [9–11] and some researchers began to use this technology to analyze the powder-binder separation [12,13], because of its obvious advantages, including 3D and the non-destructive characterization of the spatial structure. In the previous studies, powder-binder separation was analyzed by using gray value distribution in the CT reconstructed data [14,15]. However, due to the spatial resolution limit (40 μm), those results are indirect evidence to characterize this phenomenon, and the specific distribution of powder particles cannot be analyzed. In this study, a CT scan was performed by using a much higher spatial resolution to study powder-binder separation and further verifying the accuracy of previous studies.

Titanium and its alloy are famous due to their relative low density, high specific strength and corrosion resistance [16]. Because of these advantages, this material has attracted attention for many years. However, due to high processing costs, the application of titanium alloy is limited. To overcome the drawbacks of the conventional processing techniques, PIM are increasingly used to produce titanium alloy parts [17,18]. Thus, Ti6Al4V (TC4) powder was selected as the subject for this study.

The aim of this present study is a detailed quantification analysis of the powder-binder separation characteristics in the TC4 green bodies by using multiscale CT tests.

Table 1. Analysis methods of powder-binder separation in the previous studies.

Method	Description	Advantages	Limitations
Optical Microscope	observing phases distribution in the surface	visible and direct	only surface information; introducing artifacts after sample preparation
SEM	observing phases distribution in the surface	visible and direct	only surface information
Density Test	sample is broken into many parts and density distribution is obtained	high reality	introducing artifacts after sample preparation destructive tests; time consuming
Hardness Test	sample is broken into many parts and hardness distribution is obtained	high reality	destructive tests; time consuming

2. Experimental Procedure

The powder used in this study has a particle size distribution of D_{10}= 15 μm, D_{50} = 29.1 μm and D_{90} = 49.2 μm. SEM observation image and chemical information are shown in Figure 1 and Table 2, respectively. For the binder system shown in Table 3, this study used the same components and corresponding proportion as the research performed by Liu [19]. The feedstock was prepared by mixing TC4 powder (AMC Powders, Beijing, China) and binder, and the solid loading used in this study was 62 vol%. The mixture was injected into the mold cavity by using an injection pressure of 90 MPa, an injection temperature of 160 °C, and a mold temperature of 45 °C. The sample dimension is 67 mm × 11 mm × 6 mm.

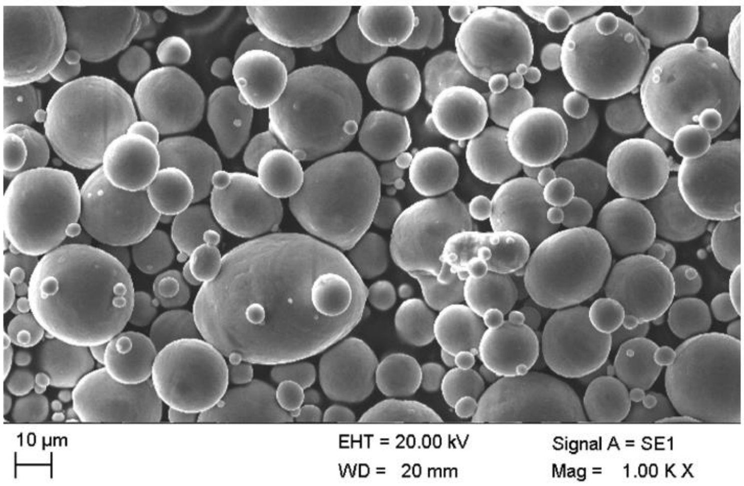

Figure 1. SEM observation of TC4 powder.

Table 2. Chemical elements of the TC4 powder.

Elements	Ti	Al	V	Fe	C	O	N
Weight (wt %)	Balance	6.14	4.13	0.09	0.011	0.092	0.0004

Table 3. Constituents of the binder.

Constituent	PW	LDPE	PP	SA	LPW	PEG-10,000	Naphthalene
Melting Point (°C)	58	125	4	66	−24	65	80.5
Binder Weight (wt %)	Balance	5–10	12	5	5–9	3	6–10

It is known that a CT test with a higher spatial resolution obtains a smaller tested area and vice-versa. To solve this problem, multiscale tests can be performed on the same sample by using a different resolution. The advantages of this method are that high resolution tested results can give clear and accurate regional information, because the structure is constituted by more voxels. For example, if a structure's volume is about 512 μm^3, for the 4 μm and 1 μm resolution tested results, the corresponding amount of voxels are 8 and 512, respectively. These data can help to speculate the structural characteristics in the whole sample tested by using a low resolution precisely. In this study, multiscale CT tests were performed on nanoVoxel-3000 equipment (Sanying Precision, Tianjin, China) which has two X-ray imaging paths. Firstly, a whole green body can be scanned by using the large view system then, for the interested areas, optical coupled with CCD system was used to perform the high resolution tests (2.3 μm and 0.8 μm). The scanning method and parameters is shown in Figure 2A and Table 4, respectively. Besides high spatial resolution, the density distinguishing ability of this system is 0.1%, thus, the subtle change of the powder contents can be distinguished precisely. Seen from Figure 2B, the regions near the gates and central part were recorded as Region 1, 2 and 3, respectively. The CT data was analyzed by Avizo 8.1 software (Thermo Fisher Scientific, Merignac, France). It is noted that every data in this paper represents a mean value of five samples.

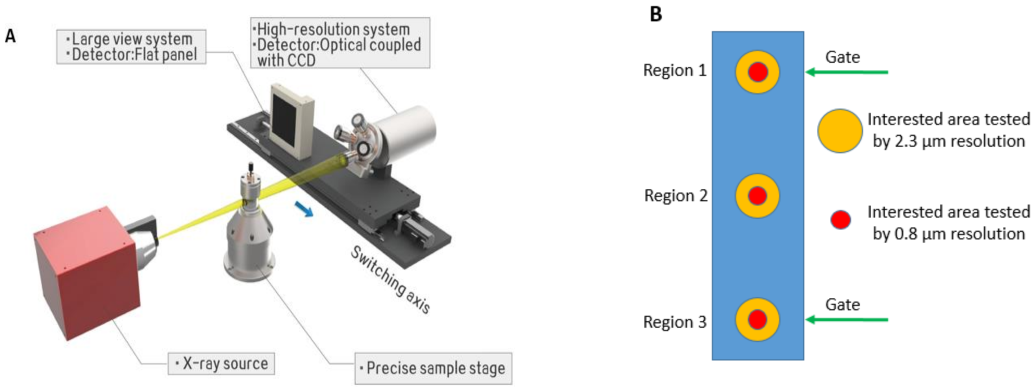

Figure 2. (**A**) Sketch map of multiscale CT tests. (**B**) Side view of the green body, the yellow and red circle shows the corresponding interested areas scanned by high resolution.

Table 4. Scanning parameters of multiscale CT tests.

Resolution (μm)	Voltage (kV)	Frames	Detector System
36	120	1440	Flat panel
2.3	120	1800	Optical coupled with CCD-4×lens
0.8	120	1800	Optical coupled with CCD-10×lens

For the X-ray CT tests, gray value of each voxel represents the corresponding matter's absorbing ability of X-ray. In Yang's study, the experiment results verified that matter's density is proportional to the gray value within certain range [14]. Moreover, in this study, to verify the accuracy of the image segmentation (OSTU method), porosities of 5 porous sample prepared by different processing were obtained by Archimedes' principle and CT data, respectively. Seen from Table 5, the results tested by the two methods are similar. Thus, the accuracy of analyzing powder-binder separation by using gray value distribution and image segmentation can be guaranteed.

Table 5. Porosity tested by Archimedes' principle and CT data.

Sample Number	Porosity Tested by Archimedes' Principle (%)	Porosity Tested by CT Data (%)
1	43.5	44.3
2	49.4	50.5
3	54.8	54.7
4	58.2	58.8
5	62.8	63.4
6	66.9	67.4

3. Results and Discussion

Firstly, powder-binder separation in the whole green body can be analyzed by using the results tested by 36 μm resolution. Figure 3A shows the reconstructed 3D rendering. Under this tested condition, it can be seen that powder particles and binder cannot be clearly distinguished, thus, the quantitative calculation of the feature structure by using threshold segmentation method cannot be used. Due to the resolution limitation, the previous study used gray value distribution to analyze powder-binder separation in the whole green body [14,15]. In this study, the average gray value of each slice image along *Z* direction was obtained. As shown by the curve in Figure 3B, the gray value increases from region 1 to region 2, then decreases from region 2 to region 3. Because the gray value is proportional to the matter density, it can be seen that powder particles and binder accumulate in the central parts and the areas near the gate, respectively, and the powder-binder separation mainly occurs in these three regions.

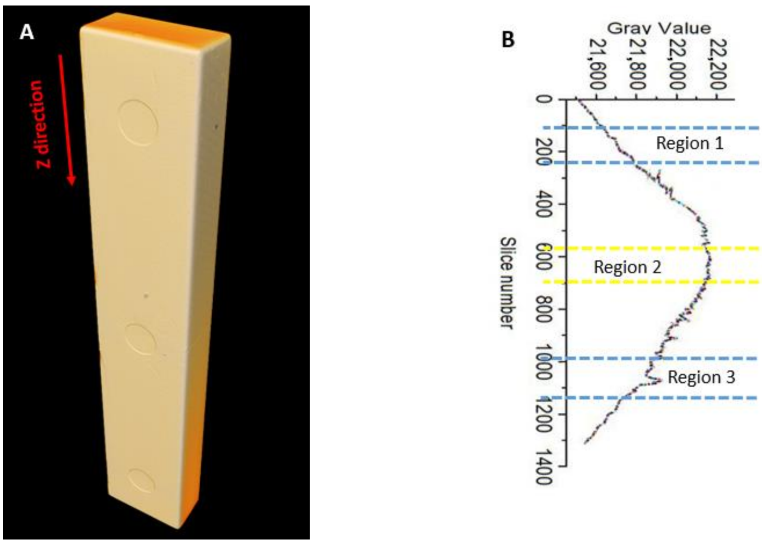

Figure 3. (**A**) 3D rendering of the whole green body. (**B**) Gray value distribution along the corresponding direction.

However, the powder-binder separation analysis by using gray value distribution is only based on the physical inferences and this method lacks direct observation results to prove its accuracy. Next, the results tested by a much higher resolution are analyzed to solve this problem.

Figure 4A shows the reconstructed slice images tested by 2.3 µm resolution and this scanned area is in the middle of the green body. It can be seen that powder particles and binder can be clearly distinguished, thus volume fraction of the corresponding structure can be calculated by the way of OSTU segmentation method. The extracted powder particles are shown in Figure 4B and the calculated volume is 600^3 voxels. Seen from Figure 4B, along *Z* direction, the average volume fraction and gray value of each slice were calculated and the results are shown in Figure 4C,D, respectively. It can be seen that the distributional characteristics of the curves are similar in the two graphs. The accuracy of the analysis method by using gray value distribution was verified by the direct observation results.

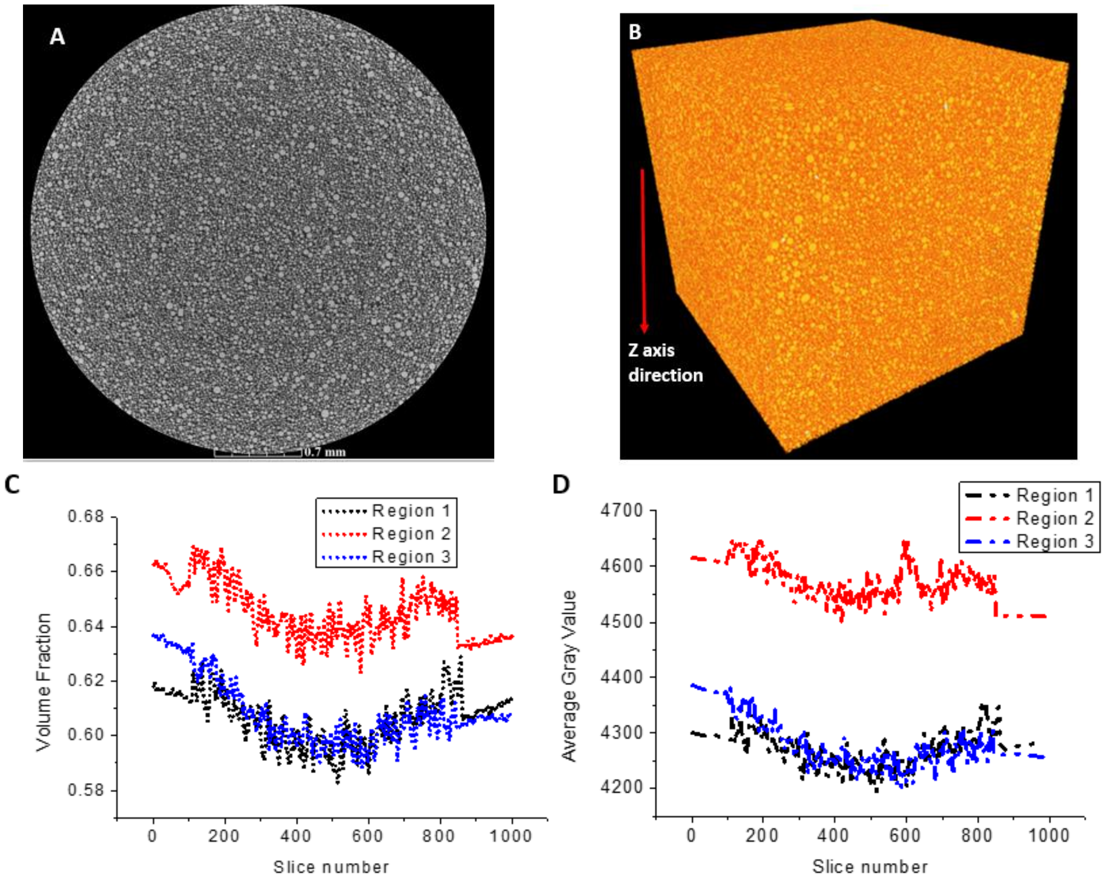

Figure 4. (**A**) Reconstructed slice image tested by 2.3 µm resolution. (**B**) The extracted powder particles in the calculated volume. (**C**) Volume fraction distribution of the powder particles along Z direction. (**D**) Gray value distribution of the slice images along Z direction. Every data point in the two figures is the mean value of 5 samples, and the relative differences calculated by each sample's data and the corresponding mean value were less than 10.6% (reasonable value for X-ray tests) and 4.3%, respectively.

Seen from Figure 4C,D, the volume fraction of powder particle and gray value of each slice in Region 2 are both higher than those of Region 1 and 3. This means that powder content tends to accumulate in the central part. In the previous studies, this phenomenon was explained by the velocity difference between the powder particles and binder during injection process. In the gate areas, shear stress for the feedstock can be very high due to the maximum shear stress usually occurs near the gate. Because the feedstock exhibits pseudo-plastic behavior, viscosity of the feedstock decreases near the gate, which may induce the powder-binder separation. Moreover, note that the ability to maintain the original velocity is related to the density of material, therefore, the velocity of powder particles was faster than that of the binder near the gates. The binder with slower velocity was surely in arrears of the powder particles, which led to more powder particles appearing in the central parts [14]. Thus, for the three regions, the different physical effects such as velocity and shearing rate lead to the different powder-binder separation phenomenon.

Seen from Figure 4C the variation range of the powder content is about 62 ± 3 vol%. According to the sintered quality of these samples, ±3% is a reasonable variation range.

To detect the more subtle phenomenon of the powder-binder separation during mold filling, the tested results of 0.8 μm resolution were analyzed. Seen from Figure 5A,B, there are many pores in the powder particles and the feature sizes can be obtained by using the measurement tool in visual analysis software. It can be seen that CT test with high resolution can also be regarded as a powerful method to evaluate the quality of powder particles.

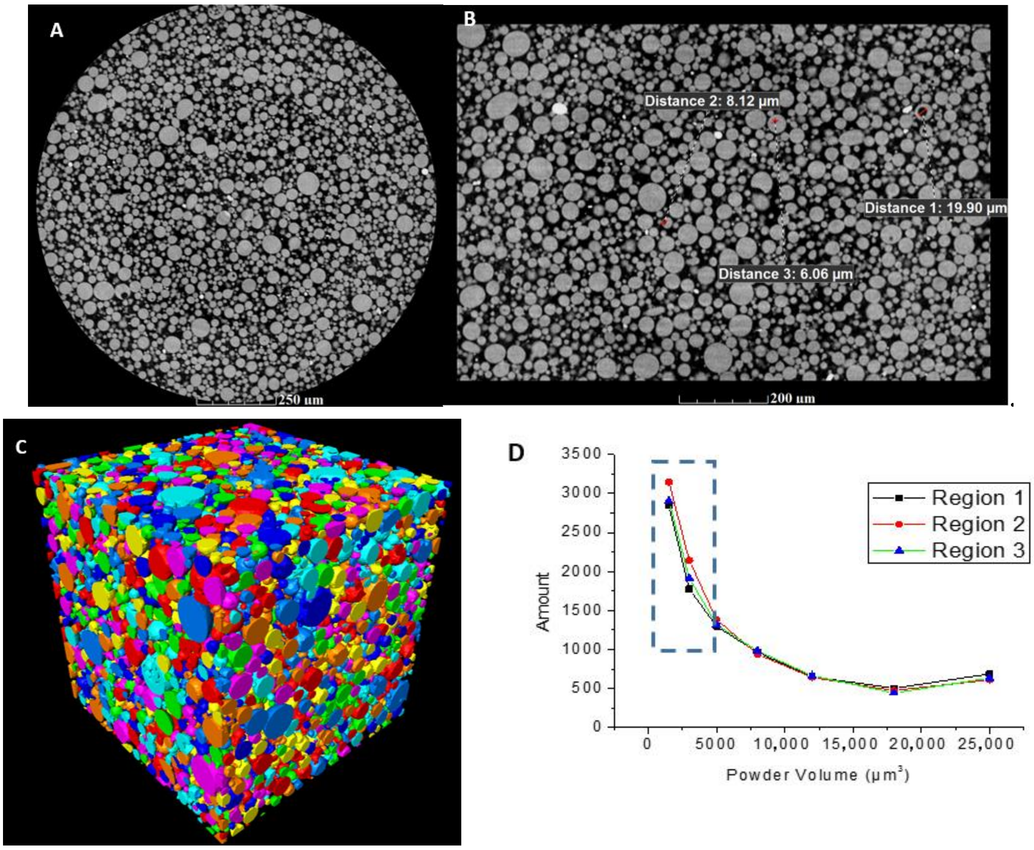

Figure 5. (**A**) Reconstructed slice image tested by 0.8 μm resolution. (**B**) Defect measurement of the powder particles. (**C**) Packing state of the powder particles. (**D**) Statistic of the powder particle volume distribution in the three local regions. Every data point in the figure is the mean value of 5 samples, and the relative differences calculated by each sample's data and the corresponding mean value were less than 4.7%.

With the resolution increasing, the micro-structure details become much more clear and the accurate morphology analysis can be performed. By the way of OSTU segmentation method, Figure 5C shows the stack state of powder particles and the size of the calculated volume is also 600^3 voxels. Firstly, the volume size of each powder particle in the three regions was calculated and the statistical results are shown in Table 6. It can be seen that a larger number of powder particles appears in the central part and the average volumes of the three regions are similar. These data can explain that why the powder content is higher in Region 2. By comparing the standard variance of the three regions in Table 6, the size of the powder particles in the central part is revealed to be more uneven. The volume distributions of powder particles in the three regions are shown in Figure 5D. The numbers of powder particle with volume larger than 5000 μm^3 are similar and there are more relatively small ones in Region 2.

Table 6. Statistical results of the volume and sphericity of the powder particles in the three local regions.

Area	Amount	Vol.		Sphericity	
		Average Volume/μm^3	Standard Deviations	Average Value	Standard Deviations
Region 1	6821	8008	13143	0.801	0.167
Region 2	7743	7749	17479	0.854	0.151
Region 3	7064	7942	14633	0.81	0.161

Based on the computational principle of 3D morphology, the sphericity degree of the powder particles were obtained and Table 6 shows the statistic results. Since this parameter of the standard sphericity is obviously 1, it can be seen that much more spherical particles appeared in the central part than in the gate area.

Combining with the statistical results obtained by the submicron resolution, in addition to the density difference between powder particles and binder, another significant factor leading to the powder binder separation is the size and shape difference of the powder particles. During mold filling, because the powder particles with relatively small volume have smaller contact surface with the other powder particles, their speeds were less affected by the friction. Moreover, for the feedstock mixture, the powder particle shape that is closer to sphere certainly has better mobility.

4. Conclusions

Multiscale CT tests provided comprehensive information for us to successfully analyze powder-binder separation phenomenon in the TC4 green bodies. Due to the density difference and shear thinning behaviors, more powder particles moved to the central parts. Based on the submicron tests (0.8 μm) results, powder particles with smaller size (volume less than 5000 μm^3) and relative spherical shape tended to accumulate in the central parts. Thus, the volume and morphology difference of the powder particles aggravated powder-binder separation. The accuracy of the analysis method used in the previous studies was verified by using the high resolution (2.3 μm) results.

Compared to the image segmentation, calculation process of the method by using gray value distribution is much easier and the demand for the test resolution is low. Thus, statistical analysis of the gray value distribution can be a more general method for the analysis of the powder-binder separation.

Author Contributions: S.Y., Q.X. and Y.X. designed the experiments; Q.X. and C.L. carried out the experiments; S.Y., X.L. and Y.X. analysed the data; X.Q. and Y.X. provided materials, instruments and analysis software; S.Y. wrote the paper under the guidance of X.L., X.Q. and Y.X.

Funding: This work was sponsored by the program of the Beijing Natural Science Foundation (No. 216053).

Acknowledgments: The authors are grateful to Wei Xu and Zheng Chen for their assistance in this work.

Conflicts of Interest: The authors declare no conflict of interest.

References

1. Enneti, R.K.; Shivashankar, T.S.; Park, S.J.; German, R.M.; Atre, S.V. Master debinding curves for solvent extraction of binders in powder injection molding. *Powder Technol.* **2012**, *228*, 14–17. [CrossRef]
2. Liu, D.M. Influence of solid loading and particle size distribution on the porosity development of green alumina ceramic moldings. *Ceram. Int.* **1997**, *23*, 513–520. [CrossRef]
3. German, R.M. *Powder Injection Molding*; Metal Powder Industries Federation: Princetion, NJ, USA, 1990.
4. Li, Y.M.; Li, L.J.; Khalil, K.A. Effect of powder loading on metal injection molding stainless steels. *J. Mater. Process. Technol.* **2007**, *183*, 432–439. [CrossRef]
5. Gelin, J.C.; Barriere, T.; Song, J. Processing defects and resulting mechanical properties after metal injection molding. *J. Eng. Mater. Technol.* **2010**, *132*, 0110171–0110179. [CrossRef]

6. Heldele, R.; Rath, S.; Merz, L.; Butzbach, R.; Hagelstein, M.; Hauβlt, J. X-ray tomography of powder injection molded micro parts using synchrotron radiation. *Nucl. Instrum. Methods Phys. Res. Sect. B Beam Interact. Mater. Atoms* **2006**, *246*, 211–216. [CrossRef]
7. Demers, V.; Fareh, F.; Turenne, S.; Demarquette, N.R.; Scalzo, O. Experimental study on moldability and segregation of Inconel 718 feedstocks used in low-pressure powder injection molding. *Adv. Powder Technol.* **2018**, *29*, 180–190. [CrossRef]
8. Thornagel, M.; Schwittay, V.; Hartmann, G. Powder-binder segregation: PIM-simulation at breakthrough. In Proceedings of the Euro PM 2014 International Conference and Exhibition, Salzburg, Austria, 21–24 September 2014; European Powder Metallurgy Association: Salzburg, Austria, 2014.
9. Tammas-Williams, S.; Withers, P.J.; Todd, I.; Prangnell, P.B. Porosity regrowth during heat treatment of hot isostatically pressed additively manufactured titanium components. *Scr. Mater.* **2016**, *122*, 72–76. [CrossRef]
10. Kurumlu, D.; Payton, E.J.; Young, M.L.; Schöbel, M.; Requena, G.; Eggeler, G. High-temperature strength and damage evolution in short fiber reinforced aluminum alloys studied by miniature creep testing and synchrotron microtomography. *Acta Mater.* **2012**, *60*, 67–78. [CrossRef]
11. Scheck, C.; Zupan, M. Ductile fracture evaluated through micro-computed X-ray tomography. *Scr. Mater.* **2011**, *65*, 1041–1044. [CrossRef]
12. Mannschatz, A.; Höhn, S.; Moritz, T. Powder-binder separation in injection moulded green parts. *J. Eur. Ceram. Soc.* **2010**, *30*, 2827–2832. [CrossRef]
13. Weber, O.; Rack, A.; Redenbach, C.; Schulz, M.; Wirjadi, O. Micropowder injection molding: Investigation of powder-binder separation using synchrotron-based microtomography and 3D image analysis. *J. Mater. Sci.* **2011**, *46*, 3568–3573. [CrossRef]
14. Yang, S.D.; Zhang, R.J.; Qu, X.H. X-ray tomographic analysis of powder-binder separation in SiC green body. *J. Eur. Ceram. Soc.* **2013**, *33*, 2935–2941. [CrossRef]
15. Yang, S.D.; Zhang, R.J.; Qu, X.H. X-ray analysis of powder-binder separation during SiC injection process in L-shaped mould. *J. Eur. Ceram. Soc.* **2015**, *35*, 61–67. [CrossRef]
16. Guo, S.B.; Qu, X.H.; He, X.B.; Zhou, T.; Duan, B.H. Powder injection molding of Ti–6Al–4V alloy. *J. Mater. Process. Technol.* **2006**, *173*, 310–314.
17. Obasi, G.C.; Ferri, O.M.; Ebel, T.; Bormann, R. Influence of processing parameters on mechanical properties of Ti–6Al–4V alloy fabricated by MIM. *Mater. Sci. Eng. A* **2010**, *527*, 3929–3935. [CrossRef]
18. Holm, M.; Ebel, T.; Dahms, M. Investigations on Ti–6Al–4V with gadolinium addition fabricated by metal injection moulding. *Mater. Des.* **2013**, *51*, 943–948. [CrossRef]
19. Liu, C.C.; Lu, X.; Yang, F.; Xu, W.; Wang, Z.; Qu, X.H. Metal Injection Moulding of High Nb-Containing TiAl Alloy and Its Oxidation Behaviour at 900 °C. *Metals* **2018**, *8*, 163. [CrossRef]